



**HAL**  
open science

## Archaeointensity study of five Late Bronze Age fireplaces from Coirent (Auvergne, France)

Gwenaël Hervé, Annick Chauvin, Pierre-Yves Milcent, Arthur Tramon

► **To cite this version:**

Gwenaël Hervé, Annick Chauvin, Pierre-Yves Milcent, Arthur Tramon. Archaeointensity study of five Late Bronze Age fireplaces from Coirent (Auvergne, France). *Journal of Archaeological Science: Reports*, 2016, 7, pp.414-419. 10.1016/j.jasrep.2016.05.018 . insu-01322354

**HAL Id: insu-01322354**

**<https://insu.hal.science/insu-01322354>**

Submitted on 27 May 2016

**HAL** is a multi-disciplinary open access archive for the deposit and dissemination of scientific research documents, whether they are published or not. The documents may come from teaching and research institutions in France or abroad, or from public or private research centers.

L'archive ouverte pluridisciplinaire **HAL**, est destinée au dépôt et à la diffusion de documents scientifiques de niveau recherche, publiés ou non, émanant des établissements d'enseignement et de recherche français ou étrangers, des laboratoires publics ou privés.

1

2 **Archaeointensity study of five Late Bronze Age fireplaces from Corent (Auvergne,**  
3 **France)**

4 Gwenaël Hervé <sup>1\*</sup>, Annick Chauvin <sup>2</sup>, Pierre-Yves Milcent <sup>3</sup>, Arthur Tramon <sup>3</sup>,

5

6 (1) Department für Geo- und Umweltwissenschaften, Ludwig-Maximilians  
7 Universität, Munich, Theresienstrasse 41, 80333 München, Germany.

8 (2) Géosciences-Rennes, UMR 6118, CNRS, Université Rennes 1, Campus de Beaulieu,  
9 35042 Rennes cedex, France.

10 (3) TRACES, UMR 5608, CNRS, Université Toulouse – Jean Jaurès, Maison de la  
11 Recherche, 5 allée Antonio Machado, 31058 Toulouse Cedex 9, France.

12 \* Corresponding author : [gherve@geophysik.uni-muenchen.de](mailto:gherve@geophysik.uni-muenchen.de)

13

14

15 **Abstract**

16 Recent excavations at Coirent (France) unearthed a vast Late Bronze Age settlement. The  
17 high density of fireplaces especially highlights it. The present study focuses on the  
18 archaeomagnetic study of five fireplaces. These ones were dated between 950 and 800  
19 BC by cross-dating of metallic and ceramic artefacts and by radiocarbon. The main  
20 objective of our study is to increase the archaeointensity database in Western Europe at  
21 the beginning of the first millennium BC. The sampling was conducted on 64 fragments  
22 of baked clay and sherds from the fireplaces floor. The classical Thellier-Thellier  
23 protocol provides 48 successful archaeointensity results, yielding to five mean values  
24 between 58 and 69  $\mu\text{T}$  at the site. Together with previously published results, our new  
25 data point out two successive maxima of the intensity of the geomagnetic field. The first  
26 maximum  $\sim 70 \mu\text{T}$  in the ninth century BC and the second  $\sim 90 \mu\text{T}$  in  $\sim 700$  BC are  
27 separated by a  $\sim 45\text{-}50 \mu\text{T}$  minimum at  $\sim 800\text{-}750$  BC. The resulting fast variation of the  
28 field intensity will be very useful for archaeomagnetic dating purposes. As the direction  
29 of the geomagnetic field has also a strong variation during this period (Hervé *et al.*,  
30 2013a), archaeomagnetism promises to be a powerful dating tool to recover the  
31 historical processes at the transition between the Bronze and Iron Ages in Western  
32 Europe.

33

34 **Keywords**

35 archaeomagnetism; archaeointensity; France; Late Bronze Age; Puy de Coirent

36

## 37 **1. Introduction**

38 The number of archaeomagnetic intensity results considerably grew in Western Europe  
39 during the last few years (e.g. Genevey et al., 2009, 2013; Gómez-Paccard et al., 2008,  
40 2012; Hervé et al., 2013b; Schnepf et al., 2009; Tema et al., 2013). Most of them cover  
41 the past 2500 years and only few have been published for older periods (Aidona et al.,  
42 2006; Gallet et al., 2009; Hervé et al., 2011; Hill et al., 2008; Kapper et al., 2015;  
43 Kovacheva et al., 2009). The latter highlight a fast secular variation in intensity,  
44 especially between 1000 and 500 BC that is at the Late Bronze Age and the Early Iron  
45 Age. This fast changing of intensity was also recovered in the Middle East (e.g. Ertepinar  
46 et al., 2012; Gallet and Le Goff, 2006; Gallet et al., 2015; Kovacheva et al., 2014; Shaar et  
47 al., 2011). A better constraint of the secular variation during this period in Western  
48 Europe will allow to better understand the geomagnetic field behaviour at the regional  
49 and global scale (Hong et al., 2013).

50 By the other hand, this fast secular variation lets also expect a great potential for the  
51 archaeomagnetic dating technique. A directional (inclination and declination) curve is  
52 already available for Western Europe (Hervé et al., 2013a). However, Western Europe  
53 intensity data for Late Bronze and Early Iron Age are still too few to build a precise and  
54 accurate regional secular variation curve. Adding the intensity to the direction will  
55 provide a more efficient chronological tool for archaeologists. The five new data from  
56 the Late Bronze Age settlement of Corent presented in this study are a new step to  
57 better recover the intensity secular variation in Western Europe and to improve the  
58 dating method for this period.

59

## 60 2. Archaeological context

61 The Puy de Corent is located on a plateau overlooking the Grande Limagne plain, 19 km  
62 away from Clermont-Ferrand in Auvergne (Latitude: 45.665°N; Longitude: 3.189°E).  
63 Since 2001, two teams of researchers have excavated this site, one from Université  
64 Lumière Lyon II conducted by Matthieu Poux and another one from Université Toulouse  
65 – Jean Jaurès conducted by Pierre-Yves Milcent. This location is very famous for its  
66 *oppidum* of the Late La Tène period, but is also characterized by earlier important  
67 agglomerations (Milcent *et al.*, 2014a and 2014b).

68 One of these important occupations of Puy de Corent's is dated at the end of the Bronze  
69 Age (from the end of the 11th to the end of 9th century BC), during which a vast and  
70 dense settlement developed on the lower part of the plateau and covered a minimum  
71 surface of 15 ha (Figure 1a). Its limits have not yet been reached and we have now some  
72 evidence that the site could be one of the first proto-urban settlements in Western  
73 Europe (Ledger *et al.*, 2015). Three successive phases of occupation and development of  
74 the agglomeration were recognized: "Bronze Final 2 récent" (~1050 – ~950 BC),  
75 "Bronze Final 3 ancien" (~950 – ~900 BC) and "Bronze Final 3 récent" (~900 – ~800  
76 BC). These phases are determined by stratigraphy. They are dated by few radiocarbon  
77 dates and by comparison of the abundant ceramics and metallic artefacts with similar  
78 objects coming from accurately dated alpine lake's palafittes. The various occupation  
79 levels display a high density of fireplaces, also dated by their relative positions in the  
80 stratigraphic sequence and according to their close relationships with the ceramic and  
81 metallic material. Radiocarbon dating (Lyon-11289, 2785±35 BP) of the occupancy level  
82 numbered [20450] related to the fireplace FY20462, assigned to "Bronze Final 3 ancien"  
83 by ceramics, confirms the archaeological dating ([950; 900] BC) with the dating interval

84 [1012; 839] BC at 95 per cent of confidence and [979; 899] BC at 68 per cent of  
85 confidence.

86 The 64 fireplaces of the Late Bronze Age (1 per 50 m<sup>2</sup> in average) discovered since 2001  
87 display, whatever their phase, some recurrent features in their shape and their  
88 construction type. Most of the time, fireplaces are built on simple or mixed raft  
89 foundation of small pebbles, basalt blocks, re-used fragments of stone macro-equipment  
90 (grindstones and granite thumb-wheels) or ceramic sherds (Figure 1b-c). They support  
91 screeds with thickness generally varying between 1 and 3 cm made of mixed clay and  
92 sand. The best-preserved fireplaces are either circular or rectangular with round angles,  
93 and measure between 1.00 and 1.60 m of diameter for the first ones, and 0.95 m x 0.70  
94 m for the latter. Repeatedly, we observed, under the raft foundation and in the center of  
95 the fireplace, a little *locus* with a depth of 5 to 10 cm and with a diameter varying from  
96 18 to 28 cm. Although they seemed sealed by the fireplace, some *loci* sheltered another  
97 deliberate deposition. The deposition are composed of bone, bronze objects (pin, ring,  
98 metal droplet) and even exceptionally a fig seed, whose the growing was limited to the  
99 Mediterranean regions at the Late Bronze Age. Positioning exactly the fireplaces in  
100 relation to the constructions on standing posts of the site remains difficult: while some  
101 were clearly inside the buildings, others seem to have been outside.

102

### 103 **3. Archaeomagnetic analyses**

#### 104 3.1 Sampling

105 We sampled five fireplaces. The best-preserved fireplaces FY20462 and FY22783  
106 (Figure 1b) were sampled *in-situ* using plaster cap method. Respectively 9 and 13 blocks

107 of baked clay were surrounded with plaster, levelled horizontally using a bubble and  
108 oriented using a magnetic compass. In the laboratory of Rennes, the baked clay  
109 fragments were prepared in 8 cm<sup>3</sup> cubic specimen after consolidation using sodium  
110 silicate. In the case of the disturbed fireplaces FY22705, FY22798 and FY22842 (Figure  
111 1c), we collected without orientation between 12 and 16 baked clay fragments and  
112 pottery sherds per structure. Those and the pottery sherds of the fireplaces FY20462  
113 and FY22783 were divided in ~1 cm<sup>3</sup> chips with the same orientation. The cutting  
114 reference was a flat side of the fragment or the sherd, which corresponded or was  
115 parallel to the surface of the fireplace. This would help to identify the component of  
116 remanent magnetization acquired *in situ*. Each chip was then packed into cylindrical  
117 quartz holder filled by quartz wool.

118

### 119 3.2 Rock magnetism

120 To investigate the ferromagnetic mineralogy, thermomagnetic curves were measured on  
121 small chips of 34 samples using a KLY3-CS3 susceptibility meter with a fitted furnace.  
122 The variation of the susceptibility was measured during heating to 400 and 600°C and  
123 during the subsequent cooling. In all baked clay fragments and pottery sherds,  
124 thermomagnetic curves reveal a dominant ferromagnetic phase with Curie  
125 temperatures between 550 and 580°C identified as titanium-poor titanomagnetite  
126 (Figure 2a-b). All heating-cooling cycles (up to 600°C) of pottery sherds are reversible  
127 (Figure 2b). On some fragments of baked clay the slight irreversibility suggests  
128 mineralogical evolutions at high temperature (Figure 2a). None samples were  
129 nevertheless rejected for archaeointensity experiments, because all cycles up to 400°C  
130 were fully reversible. Isothermal remanent magnetization (IRM) acquisition curves were

131 acquired on 21 specimens using an ASC impulse magnetizer. Saturation occurred at low  
132 magnetic fields (~300 mT), indicating the lack of any high-coercivity ferromagnetic  
133 phase (Figure 2c).

134

### 135 3.3 Thermal demagnetization

136 Prior to the archaeointensity experiment, one specimen per sample was thermally  
137 demagnetized in a Magnetic Measurement Thermal Demagnetizer (MMTD) oven, in  
138 order to identify the component of thermoremanent magnetization (TRM) acquired *in*  
139 *situ*. Sample's positions in the field suggest that the expected TRM should have an  
140 inclination of circa  $\pm 60-70^\circ$ , as based on the data from the neighbour and  
141 contemporaneous site of Lignat (Gallet et al., 2002; Moutmir, 1995).

142 Almost all (50/54) fragments of backed clay from the upper layer of the fireplaces carry  
143 a single TRM component with the expected inclination. Three pottery sherds carry two  
144 clear components of magnetization. The low-temperature component between 100 and  
145 400-500°C has a  $\sim 60-70^\circ$  inclination and was therefore acquired *in situ*. Directions of  
146 the high-temperature component are totally dispersed and they are probably associated  
147 to the initial firing of the pottery. As these three sherds were found below the baked clay  
148 layer, they reached a lower temperature during the last heating of the fireplace and  
149 therefore they carry two components of magnetization. Six pottery sherds (three from  
150 FY22798 and three from FY22842) and four baked clay samples (from FY 22798) have a  
151 multiple component magnetization, none of them close to the expected inclination. We  
152 did not perform archaeointensity experiment on these ten samples.



153 Oriented block samples from FY20462 and FY22783 carry a TRM with an easterly  
154 declination and an inclination in the range of the expected values for the Late Bronze  
155 Age (Hervé *et al.*, 2013a) (Figure 3). However the scatter between directions indicates  
156 slight displacements of the baked clay fragments since the last high-temperature heating  
157 and prevents the calculation of a mean direction of magnetization.

158

### 159 3.4 Archaeointensity study

160 Archaeointensity experiments were performed using the classical Thellier-Thellier  
161 method (Thellier and Thellier, 1959) with partial thermoremanent magnetization  
162 (pTRM) checks on 56 specimens (50 baked clay fragments and 6 pottery sherds). At  
163 each temperature step, specimens were heated and cooled twice, first in a laboratory  
164 field  $+F_{lab}$  and secondly in the opposite field  $-F_{lab}$  of 60  $\mu$ T. The protocol was performed  
165 using 13 temperature steps up to 570 or 580°C in a Pyrox amagnetic oven. All remanent  
166 magnetization were measured with a 2G cryogenic magnetometer. The anisotropy of  
167 TRM was determined at 510 or 540°C using 6 successive heating and one stability check  
168 (Chauvin *et al.*, 2000). The cooling rate effect on TRM intensity was also corrected at 535  
169 or 555°C using the procedure in four heating steps of Gómez-Paccard *et al.* (2006). The  
170 slow cooling rate was fixed to 8 hours.

171 We used the following criteria to select the specimens for the mean archaeointensity  
172 calculation: NRM fraction factor higher than 0.5, maximum angular deviation  $Mad$  lower  
173 than 5°, deviation angle  $Dang$  lower than 5° and ratio of the standard error of the slope  
174 to the absolute value of the slope  $\beta$  lower than 0.05. A pTRM-check was said positive if  
175 its difference with the original pTRM was lower than 10%. Samples showing a concave-

176 up NRM-TRM diagram indicating some mineralogical changes during heating were  
177 rejected from the analysis (Figure 4a). All the accepted specimens have a linear NRM-  
178 TRM diagram (Figure 4b). In the case of pottery sherds, the archaeointensity was  
179 computed using the secondary component of magnetization after correction of the NRM-  
180 TRM diagram (Hervé et al., 2013b, Figure 4c). The selection procedure yields an  
181 acceptance rate of 86% (Supplementary material).

182 The archaeointensity values were corrected for TRM anisotropy if the alteration factor  
183 inferred from the stability check was lower than 10%. The anisotropy degree varied  
184 from 3 to 27%. The cooling rate correction was applied only when the absolute value of  
185 the correction factor was higher than the alteration factor (Gómez-Paccard et al., 2006).  
186 Otherwise, that is for ten specimens, the cooling rate correction was not accounted for.  
187 The correction factor was usually lower than 6%, except for specimens from FY20462  
188 with values between 10 and 15%. The mean archaeointensity per fireplace was  
189 computed using the weighting method of Prévot et al. (1985) (Table 1). The five mean  
190 values agree well with each other.

191

#### 192 **4. Discussion**

193 Our new mean archaeointensities were relocated to Paris using the Virtual Axial Dipole  
194 Moment (VADM) correction. On Figure 5, they are compared to published Western  
195 European data for Late Bronze and Iron Ages. These data include the selected data set  
196 described in Hervé et al., (2013b) completed by new Swiss data (in grey on Figure 5,  
197 Kapper et al., 2015). Given the small number of published results, the five fireplaces of  
198 Corent represent a significant step to recover the secular variation of the geomagnetic

199 field intensity between 1500 and 600 BC. The large range of archaeointensities (~50-  
200 90 $\mu$ T) between 1000 and 600 BC points out high and fast variations of the geomagnetic  
201 field strength.

202 An increase of the field intensity is observed during the tenth century BC up to ~65-70  
203  $\mu$ T, followed by a possible decrease during the ninth century with values close to 45  $\mu$ T  
204 at ~800-750 BC. After that, the intensity would increase up to ~90  $\mu$ T in ~700-600 BC, as  
205 supported by Gallet et al. (2009), Hervé et al. (2011) and Hill et al. (2008) data.

206 From ~800 to ~700-600 BC, the secular variation rate would have been around ~3  
207  $\mu$ T/decade. This rate is higher than the typical one (1  $\mu$ T/decade) observed over the last  
208 two millennia in Western Europe (Genevey et al., 2013) but is similar to the rate during  
209 the early Middle Age (Gómez-Paccard et al., 2012). The sharp secular variation at the  
210 beginning of the Early Iron Age may be recorded in the Swiss mean data with an unusual  
211 standard deviation of 15.5  $\mu$ T (Kapper et al., 2015, grey triangle data on Figure 5). This  
212 average archaeointensity was computed from two pottery sherds coming from the same  
213 archaeological layer. They provide archaeointensities of 45 and 75  $\mu$ T. We suggest that  
214 these potteries were magnetized at slightly different times during a period of fast  
215 changes of the field intensity.

216 The Corent data do not record the geomagnetic spikes (short-lived high field anomalies),  
217 highlighted in the Levantine area during the ninth century BC (Ben-Yosef et al., 2009;  
218 Shaar et al., 2011). Other new reference data are needed to investigate the presence of  
219 such events in Western Europe and to better estimate the secular variation rate during  
220 the Late Bronze Age.

221 Finally, our new data are compared to the prediction at Paris of the geomagnetic model  
222 SHA.DIF.14k that is valid in the Northern hemisphere (Figure 5)(Pavón-Carrasco et al.,  
223 2014a). This model is developed by inversion of archaeomagnetic and volcanic results  
224 using spherical harmonic analysis in space and penalised cubic B-splines in time. For the  
225 1500-500 BC time period the data set used to build the model includes a large amount of  
226 results obtained on Eastern Europe sites. All the data in black on Figure 5 are also used  
227 to build the SHA.DIF.14k model but not the more recently published Swiss data in grey  
228 (Kapper et al., 2015). The SHA.DIF.14k model's prediction does not fit well most of the  
229 data between 1000 and 500 BC. Maxima of intensity are observed but with shifts in time  
230 and amplitude compared to Western Europe archaeointensity results. The  
231 archaeointensity values obtained at Corent are higher than the model's prediction and  
232 differ up to 15  $\mu$ T. Inhomogeneous quality of the archaeointensities and inhomogeneous  
233 geographical distribution of sites in the global database probably explains these  
234 inconsistencies (Pavón-Carrasco et al., 2014b). Finally this comparison indicates that  
235 reliable intensity data are still needed in order to better constrain global models of the  
236 past geomagnetic field.

237

## 238 **5. Conclusion**

239 The study of fireplaces from the archaeological site Puy de Corent provides five new  
240 high quality archaeointensities at the Late Bronze Age in Western Europe. This  
241 represents a new step to increase the amount of reliable data set and to build a  
242 reference curve of the secular variation of the geomagnetic field intensity. The large and  
243 fast secular variation at the Late Bronze Age and the Early Iron Age lets expect that this  
244 reference curve will give precise archaeomagnetic dating both for in place and displaced

245 objects. Together with directional data of the geomagnetic field, which also shows large  
246 variations, archaeomagnetic dating technique will provide a very valuable alternative to  
247 radiocarbon, especially problematic during this period due to plateau effects.  
248 Archaeomagnetism will efficiently contribute to the refinement of our knowledge of the  
249 evolutions of the societies in Western Europe at the transition from the Bronze Age to  
250 the Iron Age.

251

## 252 **Acknowledgements**

253 GH thanks the Deutsches Forschung Gemeinschaft for funding (project HE7343/1-1).  
254 Philippe Cullerier is kindly acknowledged for his help in sample's preparation and  
255 Thellier-Thellier measurements. We thank an anonymous reviewer for his/her  
256 insightful review.

257

## 258 **References**

- 259 Aidona, E., Scholger, R., Mauritsch, H.J., Schnepf, E., Klemm, S., 2006. Spatial distribution  
260 of archaeomagnetic vectors within archaeological samples from Eisenerz (Austria).  
261 *Geophys. J. Int.* 166, 46–58. doi:10.1111/j.1365-246X.2006.02944.x
- 262 Ben-Yosef, E., Tauxe, L., Levy, T.E., Shaar, R., Ron, H., Najjar, M., 2009. Geomagnetic  
263 intensity spike recorded in high resolution slag deposit in Southern Jordan. *Earth Planet.*  
264 *Sci. Lett.* 287, 529–539. doi:10.1016/j.epsl.2009.09.001

265 Chauvin, A., Garcia, Y., Lanos, P., Laubenheimer, F., 2000. Paleointensity of the  
266 geomagnetic field recovered on archaeomagnetic sites from France. *Phys. Earth Planet.*  
267 *Inter.* 120, 111–136.

268 Ertepinar, P., Langereis, C.G., Biggin, A.J., Frangipane, M., Matney, T., Ökse, T., Engin, A.,  
269 2012. Archaeomagnetic study of five mounds from Upper Mesopotamia between 2500  
270 and 700 BCE: Further evidence for an extremely strong geomagnetic field ca. 3000 years  
271 ago. *Earth Planet. Sci. Lett.* 357-358, 84–98. doi:10.1016/j.epsl.2012.08.039

272 Gallet, Y., Le Goff, M., 2006. High-temperature archeointensity measurements from  
273 Mesopotamia. *Earth Planet. Sci. Lett.* 241, 159–173. doi:10.1016/j.epsl.2005.09.058

274 Gallet, Y., Genevey, A., Le Goff, M., 2002. Three millennia of directional variation of the  
275 Earth's magnetic field in western Europe as revealed by archeological artefacts. *Phys.*  
276 *Earth Planet. Inter.* 131, 81–89. doi:10.1016/S0031-9201(02)00030-4

277 Gallet, Y., Genevey, A., Le Goff, M., Warmé, N., Gran-Aymerich, J., Lefèvre, A., 2009. On  
278 the use of archeology in geomagnetism, and vice-versa: Recent developments in  
279 archeomagnetism. *Comptes Rendus Phys.* 10, 630–648. doi:10.1016/j.crhy.2009.08.005

280 Gallet, Y., Molist, M., Genevey, A., Clop, X., Thébault, E., Gómez, A., Le, M., Robert, B.,  
281 Nachasova, I., 2015. New Late Neolithic (c . 7000 – 5000 BC) archeointensity data from  
282 Syria. Reconstructing 9000 years of archeomagnetic field intensity variations in the  
283 Middle East. *Phys. Earth Planet. Inter.* 238, 89–103. doi:10.1016/j.pepi.2014.11.003

284 Genevey, A., Gallet, Y., Rosen, J., Le Goff, M., 2009. Evidence for rapid geomagnetic field  
285 intensity variations in Western Europe over the past 800 years from new French

286 archeointensity data. *Earth Planet. Sci. Lett.* 284, 132–143.  
287 doi:10.1016/j.epsl.2009.04.024

288 Genevey, A., Gallet, Y., Thébault, E., Jesset, S., Le Goff, M., 2013. Geomagnetic field  
289 intensity variations in Western Europe over the past 1100 years. *Geochemistry,*  
290 *Geophys. Geosystems* 14, 2858–2872. doi:10.1002/ggge.20165

291 Gómez-Paccard, M., Chauvin, A., Lanos, P., Thiriot, J., Jiménez-Castillo, P., 2006.  
292 Archeomagnetic study of seven contemporaneous kilns from Murcia (Spain). *Phys.*  
293 *Earth Planet. Inter.* 157, 16–32. doi:10.1016/j.pepi.2006.03.001

294 Gómez-Paccard, M., Chauvin, A., Lanos, P., Thiriot, J., 2008. New archeointensity data from  
295 Spain and the geomagnetic dipole moment in western Europe over the past 2000 years. *J.*  
296 *Geophys. Res.* 113, B09103. doi:10.1029/2008JB005582

297 Gómez-Paccard, M., Chauvin, A., Lanos, P., Dufresne, P., Kovacheva, M., Hill, M.J.,  
298 Beamud, E., Blain, S., Bouvier, A., Guibert, P., 2012. Improving our knowledge of rapid  
299 geomagnetic field intensity changes observed in Europe between 200 and 1400 AD.  
300 *Earth Planet. Sci. Lett.* 355–356, 131–143. doi:10.1016/j.epsl.2012.08.037

301 Hervé, G., Schnepf, E., Chauvin, A., Lanos, P., Nowaczyk, N., 2011. Archaeomagnetic  
302 results on three Early Iron Age salt-kilns from Moyenvic (France). *Geophys. J. Int.* 185,  
303 144–156. doi:10.1111/j.1365-246X.2011.04933.x

304 Hervé, G., Chauvin, A., Lanos, P., 2013a. Geomagnetic field variations in Western Europe  
305 from 1500BC to 200AD. Part I: Directional secular variation curve. *Phys. Earth Planet.*  
306 *Inter.* 218, 1–13. doi:10.1016/j.pepi.2013.02.002

- 307 Hervé, G., Chauvin, A., Lanos, P., 2013b. Geomagnetic field variations in Western Europe  
308 from 1500 BC to 200 AD. Part II: New intensity secular variation curve. *Phys. Earth  
309 Planet. Inter.* 218, 51–65. doi:10.1016/j.pepi.2013.02.003
- 310 Hill, M.J., Lanos, P., Denti, M., Dufresne, P., 2008. Archaeomagnetic investigation of bricks  
311 from the VIIIth–VIIth century BC Greek–indigenous site of Incoronata (Metaponto,  
312 Italy). *Phys. Chem. Earth, Parts A/B/C* 33, 523–533. doi:10.1016/j.pce.2008.02.026
- 313 Hong, H., Yu, Y., Lee, C.H., Kim, R.H., Park, J., Doh, S.-J., Kim, W., Sung, H., 2013.  
314 Globally strong geomagnetic field intensity circa 3000 years ago. *Earth Planet. Sci. Lett.*  
315 383, 142–152. doi:10.1016/j.epsl.2013.09.043
- 316 Kapper, K.L., Donadini, F., Hirt, A.M., 2015. Holocene archeointensities from mid European  
317 ceramics, slags, burned sediments and cherts. *Phys. Earth Planet. Inter.* 241, 21–36.  
318 doi:10.1016/j.pepi.2014.12.006
- 319 Kovacheva, M., Boyadziev, Y., Kostadinova-Avramova, M., Jordanova, N., 2009. Updated  
320 archeomagnetic data set of the past eight millenia from the Sofia laboratory, Bulgaria.  
321 *Geochemistry Geophys. Geosystems* 10. doi:10.1029/2008GC002347
- 322 Kovacheva, M., Kostadinova-Avramova, M., Jordanova, N., Lanos, P., Boyadzhiev, Y., 2014.  
323 Extended and revised archaeomagnetic database and secular variation curves from  
324 Bulgaria for the last eight millennia. *Phys. Earth Planet. Inter.* 236, 79–94.  
325 doi:10.1016/j.pepi.2014.07.002
- 326 Ledger, P., Miras, Y., Poux, M., Milcent, P.-Y. 2015. The Palaeoenvironmental Impact of  
327 Prehistoric Settlement and Proto-Historic Urbanism: Tracing the Emergence of the



- 328 Oppidum of Corent, Auvergne, France. *PLoS ONE*, 10(4): e0121517.  
329 doi:10.1371/journal.pone.0121517.
- 330 Milcent, P.-Y., Poux, M., Mader, S., Torres, M., Tramon, A., 2014a. Une agglomération de  
331 hauteur autour de 600 a.C. en Gaule centrale : Corent (Auvergne). *In* : Alberti G., Féliu  
332 Cl., Pierrevelcin G. (eds.) *Transalpinare. Mélanges offerts à Anne-Marie Adam*,  
333 Ausonius Editions, Collection Mémoires, 36, Bordeaux, 2014, 181-204.
- 334 Milcent, P.-Y., Chassan, N., Mader, S., Saint-Sever, G., Tramon, A., 2014b. Les occupations  
335 de l'âge du Bronze du plateau de Corent (Auvergne, Puy-de-Dôme) : résultats des  
336 campagnes de fouille 2010-2013. *Bull. de l'APRAB*, 12, 89-94.
- 337 Moutmir, A., 1995. Analyses magnétiques de terres cuites protohistoriques en France.  
338 Apports en archéomagnétisme (Premier millénaire avant J.-C.) et en archéologie.  
339 Muséum National d'histoire Naturelle, Paris.
- 340 Pavón-Carrasco, F.J., Osete, M.L., Torta, J.M., De Santis, A., 2014a. A geomagnetic field  
341 model for the Holocene based on archaeomagnetic and lava flow data, *Earth Planet. Sci.*  
342 *Lett.* 388, 98-109.
- 343 Pavón-Carrasco, F.J., Gomez-Paccard, M., Hervé, G., Osete, M.L., Chauvin, A., 2014b.  
344 Intensity of the geomagnetic field in Europe for the last 3 ka: Influence of data quality on  
345 geomagnetic field modeling. *Geochemistry Geophys. Geosystems* 1–16.  
346 doi:10.1002/2014GC005311
- 347 Prévot, M., Mankinen, E.A., Coe, R.S., Grommé, C.S., 1985. The Steens Mountain (Oregon)  
348 geomagnetic polarity transition, 2. Field intensity variations and discussion of reversal  
349 models. *J. Geophys. Res.* 90, 10417–10448.

350 Schnepf, E., Lanos, P., Chauvin, A., 2009. Geomagnetic paleointensity between 1300 and  
351 1750 A.D. derived from a bread oven floor sequence in Lübeck, Germany.  
352 *Geochemistry, Geophys. Geosystems* 10, doi:10.1029/2009GC002470

353 Shaar, R., Ben-Yosef, E., Ron, H., Tauxe, L., Agnon, A., Kessel, R., 2011. Geomagnetic field  
354 intensity: How high can it get? How fast can it change? Constraints from Iron Age  
355 copper slag. *Earth Planet. Sci. Lett.* 301, 297–306. doi:10.1016/j.epsl.2010.11.013

356 Tema, E., Morales, J., Goguitchaichvili, A., Camps, P., 2013. New archaeointensity data from  
357 Italy and geomagnetic field intensity variation in the Italian Peninsula. *Geophys. J. Int.*  
358 193, 603–614. doi:10.1093/gji/ggs120

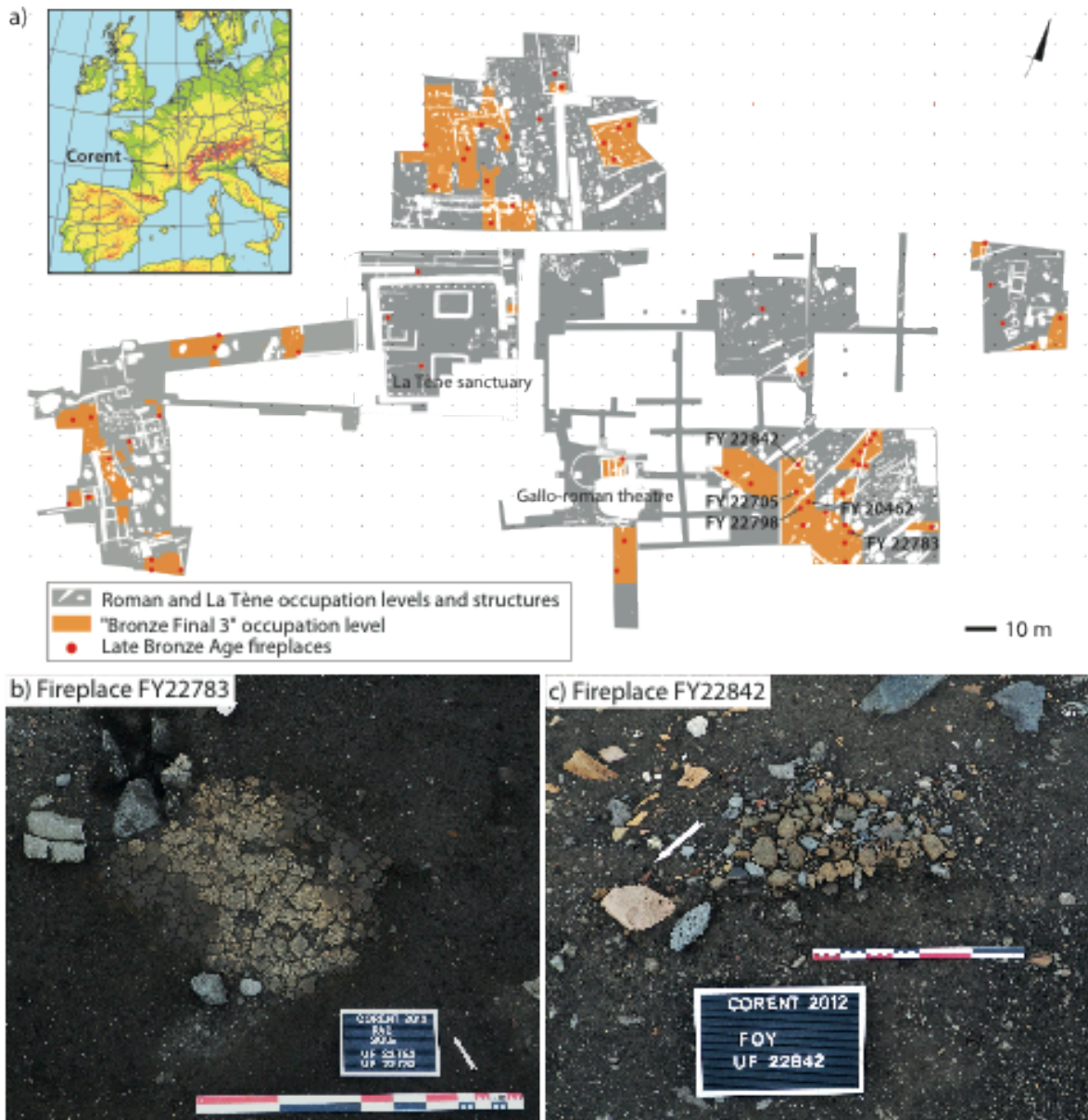
359 Thellier, E., Thellier, O., 1959. Sur l'intensité du champ magnétique terrestre dans le passé  
360 historique et géologique. *Ann. Géophysique* 15, 285–376.

361

362

363

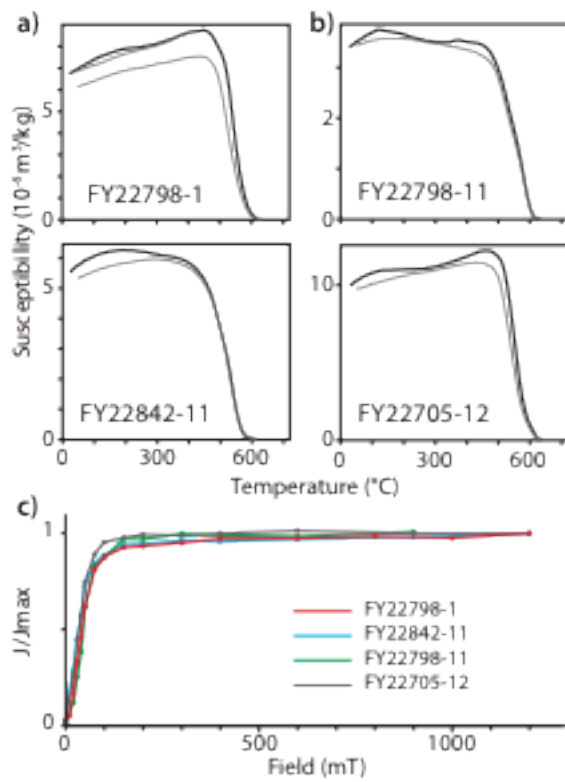
364 Figure 1: Map of the central area of Corent archaeological site (2001 to 2015  
365 excavations) emphasizing the levels from the Late Bronze Age ("Bronze Final 3") and  
366 their associated fireplaces (a) and pictures of two sampled fireplaces (b-c).



367

368

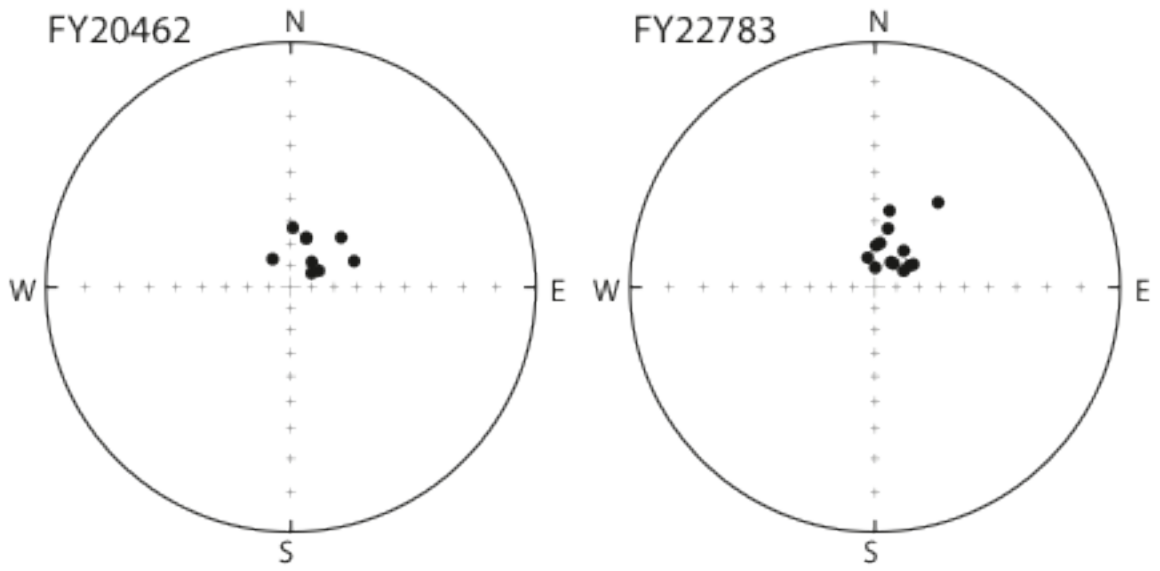
369 Figure 2: Representative magnetic mineralogy results with thermomagnetic curves of  
370 baked clay fragments (a) and of pottery sherds (b) together with acquisition curves of  
371 isothermal remanent magnetization (c). In thermomagnetic curves, the black curve is  
372 the variation of susceptibility during the heating and the grey curve during the cooling.



373

374

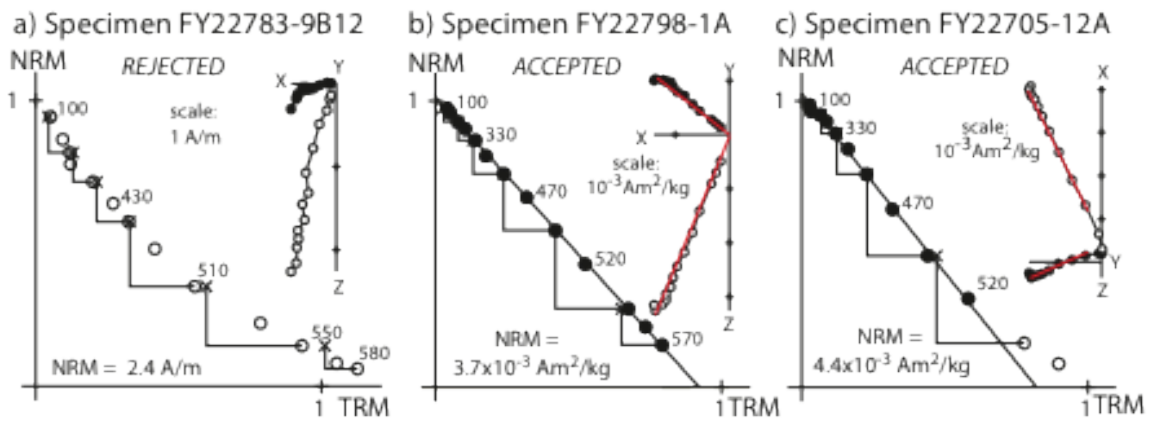
375 Figure 3: Stereographic plot of the TRM directions obtained on oriented block samples  
376 from FY20462 and FY22783 fireplaces.



377

378

379 Figure 4: Archaeointensity results of baked clay fragments (a-b) and of pottery sherds  
 380 (c). Solid circles on NRM-TRM diagrams indicate the temperature steps used in the  
 381 intensity determination. Corresponding demagnetization directions are shown in  
 382 sample coordinates in the orthogonal diagrams. Open (solid) circles denote the  
 383 projection on the vertical (horizontal) plane.

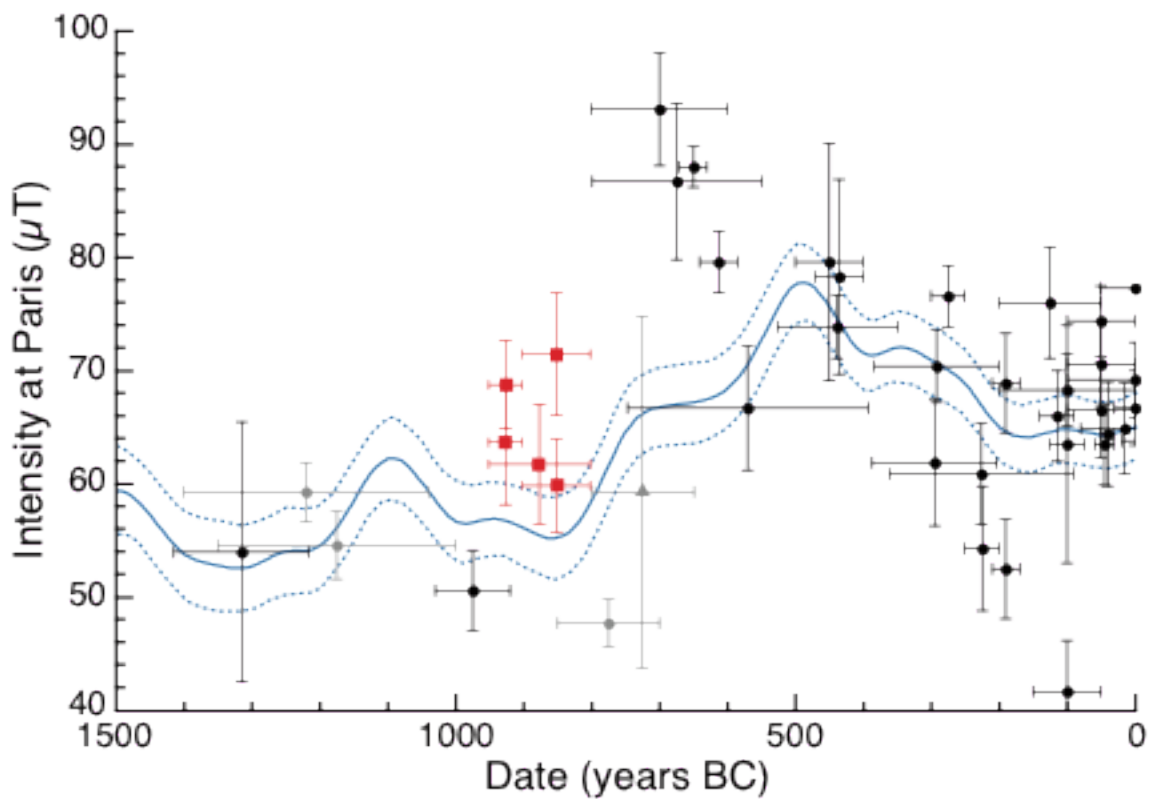


384

385

386 Figure 5: Secular variation of the geomagnetic intensity at the Late Bronze and Iron Ages  
387 in Western Europe. Corent data (red squares) are plotted with other published data  
388 (black squares represent the selection of Hervé et al. 2013b, whereas gray circles and  
389 triangles are the Swiss data of Kapper et al. 2015). The gray triangle indicates the Swiss  
390 data with an unusual standard deviation discussed in the text. All data are relocated to  
391 Paris. The blue curve is the mean intensity with its 95 per cent confidence envelop  
392 predicted by the geomagnetic model SHA.DIF.14k (Pavón-Carrasco et al., 2014). The  
393 Swiss data in grey are not included in this model.

394



395

396

397 Table 1: Archaeological dating and mean archaeointensities of studied fireplaces.  
 398 Fireplace, name of the sampled structure; Age, dating interval in years BC of the last use  
 399 of the fireplace; N, number of specimens used in the calculation of the structure mean  
 400 archaeointensity;  $F \pm SD$ , mean raw archaeointensity and standard deviation;  $F_a \pm SD$ ,  
 401 mean archaeointensity and standard deviation corrected for TRM anisotropy;  $F_{a+c} \pm SD$ ,  
 402 mean archaeointensity and standard deviation corrected for TRM anisotropy and  
 403 cooling rate;  $F_{Paris}$ , mean archaeointensity relocated to Paris using Virtual Axial Dipole  
 404 Moment correction.

Fireplace	Age (BC)	N	$F \pm SD$ ( $\mu T$ )	$F_a \pm SD$ ( $\mu T$ )	$F_{a+c} \pm SD$ ( $\mu T$ )	$F_{Paris}$ ( $\mu T$ )
FY20462	[950; 900]	8	$69.7 \pm 5.6$	$70.3 \pm 5.7$	$61.6 \pm 5.5$	63.6
FY22783	[950; 900]	12	$65.2 \pm 3.1$	$69.0 \pm 3.8$	$66.5 \pm 3.9$	68.7
FY22798	[900; 800]	6	$62.5 \pm 5.5$	$60.7 \pm 4.0$	$57.9 \pm 4.1$	59.8
FY22705	[900; 800]	12	$71.5 \pm 4.5$	$71.6 \pm 4.8$	$69.2 \pm 5.4$	71.4
FY22842	[950; 800]	10	$60.5 \pm 4.8$	$60.8 \pm 5.0$	$59.7 \pm 5.3$	61.7

405

406